

Simulation and Optimization of a Multistage Interconnected Fluidized Bed Reactor for Coal Chemical Looping Combustion

Xiao Zhu, Rong Wang, Tianxu Shen, and Laihong Shen*

Cite This: *ACS Omega* 2022, 7, 40990–41000

Read Online

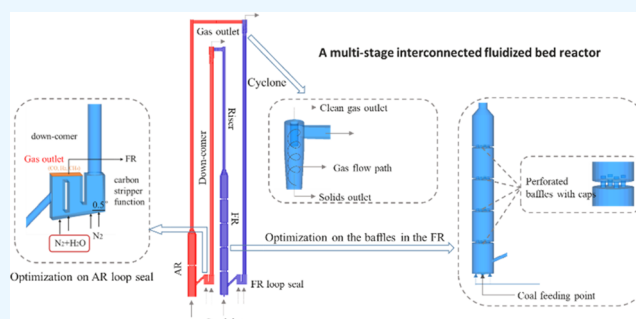
ACCESS |

Metrics & More

Article Recommendations

Supporting Information

ABSTRACT: This work established a three-dimensional model of a chemical looping system with multistage reactors coupled with hydrodynamics and chemical reactions. The thermal characteristics in the chemical looping combustion (CLC) system were simulated using coal as fuel and hematite as an oxygen carrier (OC). Some significant aspects, including gas composition, particle residence time, backmixing rate, wall erosion, carbon capture rate, etc., were investigated in the simulation. Owing to the optimization by adding baffles in the fuel reactor (FR), the gas conversion capacity of the multistage FR was high, where the outlet CO₂ concentration was as high as 93.8% and the oxygen demand was as low as 3.8%. Through tracing and analyzing the path of char particles, we found that the residence time of most char particles was too short to be fully gasified. The residual char will be entrained into the air reactor (AR), reducing the CO₂ capture rate, which is only 80.3%. In the simulation, the wall erosion on the cyclone could be relieved by increasing the height of the horizontal pipe. In addition, improving the structure of the AR loop seal could control the residual char entrained by OC particles to the AR, and the CO₂ capture rate was increased up to 90% in the multistage CLC reactor.



1. INTRODUCTION

Nowadays, the emission of greenhouse gases keeps increasing and global warming has become severe, which harms the ecosystem.¹ The depletion in the reserves of fossil fuel resources and the demands of reducing CO₂ emissions have driven worldwide efforts to develop efficient and reliable carbon capture and storage (CCS) technologies for CO₂ emissions.² Chemical looping combustion (CLC) is one of the most promising routes for green, low-cost, sustainable, and safe conversion technology based on the merit of inherent CO₂ separation during carbonaceous fuel conversion. A metal oxide is used as an oxygen carrier (OC) to complete the orderly redox cycle between the fuel reactor (FR) and air reactor (AR). The fuel is not in direct contact with air, and the separation of CO₂ can be realized through simple condensation. The separation strategy can decrease the energy penalty and improve the exergy efficiency.^{3–5}

In situ gasification chemical looping combustion (iG-CLC) has been regarded as one of the solid-fueled CLC technologies.⁶ In the FR, the direct reactions between the coal and the OC are avoided, and no additional gasification device is required. Typically, the iG-CLC process employs a dual circulating fluidized bed reactor to flexibly control the solid circulation rate.^{7,8} However, some limitations have been reported in the CLC process, including incomplete gas–solid contact, low combustion efficiency, and low carbon capture.^{9–11} These problems also existed in an MW_{th} CLC pilot.¹² Several kinds of strategies have been proposed to address these

issues, as summarized in Figure 1. Thon et al.¹³ employed a two-stage FR to improve fuel conversion. The secondary reactor showed good chemical reaction performance; however, unconverted char particles were easily carried from the bottom chamber into the upper chamber. At the same time, some combustible gases were easy to escape from the downcomer, resulting in gas leakage between reactors. Pröll et al.¹⁴ proposed a circulating fluidized bed fuel reactor with annular internals to extend the FR's particle residence time. The results showed that more combustible gases were wholly converted in the FR, and the combustion efficiency was improved. However, adding annular internals would increase the load of the whole reactor system, and severe erosion existed on the internal surface. Adding a cyclone separator¹⁵ and enlarging coal particle size⁹ were feasible strategies for high combustion efficiency but also led to disadvantages like low fuel adaptability and complex reactor structure. Improving CO₂ capture efficiency is the goal of each CLC reactor. According to the experimental results by Pérez-Vega et al.,¹⁶ the carbon capture rate could be increased from 63 to 89% when the

Received: July 4, 2022

Accepted: October 17, 2022

Published: November 6, 2022



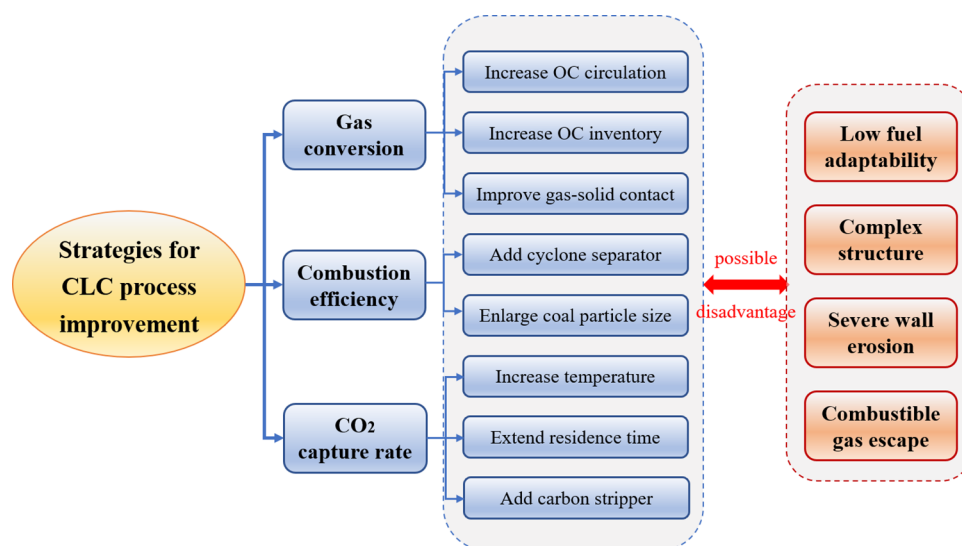


Figure 1. Strategies for CLC process improvement and possible disadvantages.

temperature of the FR was increased from 903 to 990 °C. However, blindly pursuing a high temperature would lead to operation risks for the system, which increased the sintering probability of OC particles and broke the thermal balance between reactors. Adding a carbon stripper is also an effective method to improve CO₂ capture. Markström et al.^{7,17} first coupled a carbon stripper in the 100kW_{th} chemical looping combustion of solid fuels and realized the CO₂ capture rate up to 99%. Due to the difference in the size and density of char and OC particles, their effective separation was realized. However, the additional particle circulation paths significantly increased the reactor's structural complexity and operation difficulty. In addition, an optimization by adding oxygen in a postoxidation chamber downstream of the FR (oxy-polishing) was applied in the design of a 1000 MW_{th} boiler¹⁸ for higher CO₂ capture and fuel conversion. Hence, the investigation of the optimization method of a CLC device is necessary.

Focusing on the need for wide fuel adaptability and flexible operation for chemical looping combustion, a 3 kW_{th} interconnected fluidized bed reactor was established in our studies with the design criteria of simple circulation structure and efficient conversion.^{19,20} The chemical looping device was optimized by adding internal baffles in the fuel reactor to intensify gas–solid contact. In a traditional bubbling fluidized bed, large bubbles and nonuniformity of particle distribution would lead to insufficient gas–solid contact, reduce reaction efficiency, and exacerbate the wear of the bed structure. However, in the multistage fluidized bed with baffles, the gas–solid contact was intensified by reconstructing the fluidization and prolonging the particle residence time. The AR was also improved into a two-stage bubbling bed for sufficient gas–solid mixing and high heat/mass transfer efficiency. In addition, the FR loop seal can be optimized to get a higher CO₂ capture rate based on the U-type structure. The improved FR loop seal can be used as a carbon stripper with a simple design for preventing the unconverted char particles from entering the AR. The results are of great significance to exploring the combustion reaction mechanism, guiding the operation parameters, and understanding the feasibility of the practical operation.

However, the limitation of experimental measurements makes it difficult to obtain the inner characteristics of the

reaction phenomenon in detail. The coal CLC process includes complex physical and chemical reactions, which aggravates the difficulty of experimental research. Computational particle fluid dynamics (CPFD)^{21,22} has excellent advantages in chemical reaction simulations at the particle level. The chemical reaction during the interaction between particles and the fluid is closely related to particle concentration, size, fluid temperature, and pressure. Combined with the basic theory of chemical reaction dynamics, the CPFD method can simulate the chemical reaction at the particle level to obtain the spatial distribution of many significant parameters at each position and each time. Hence, a further study on the multistage interconnected fluidized bed is realized. At present, plenty of studies have employed the CPFD method in the multiphase flow, including bubbling bed,²³ spouted bed,²⁴ and circulating bed.²⁵ The relatively reasonable results have proved the feasibility of the CPFD simulations. However, the works applying CPFD in the CLC process are pretty few to date. Parker et al.²⁶ simulated the CLC process by CPFD, obtaining the temperature distribution and component characteristics of the entire device and further improving the accuracy of CLC simulations. In addition, Chen et al.²⁷ established a 50 kW_{th} dual circulating fluidized bed model based on CPFD simulations, which can help to optimize the reactor configuration and eventually achieve reliable prediction of the reactor in an effective way.

The paper established a three-dimensional (3D) numerical model for a multistage interconnected fluidized bed system in the coal-fueled CLC process. Several aspects, including the gas product distribution, particle residence time, and backmixing rate, were simulated to illustrate the optimization effect of baffles in the FR. The following properties were evaluated: combustion efficiency, oxygen demand, and carbon capture rate. The AR loop seal structure was also optimized for a higher CO₂ capture rate. In addition, the study further discussed the erosion in the CLC device. Based on the optimization of gas–solid contact and char residence time, better performance of the CLC unit was achieved.

2. METHODOLOGY AND PROCEDURE

2.1. Simulation Model. The CPFD approach is based on software Barracuda. The governing equations of the fluid and particle in the simulation are listed in Table S1 in the

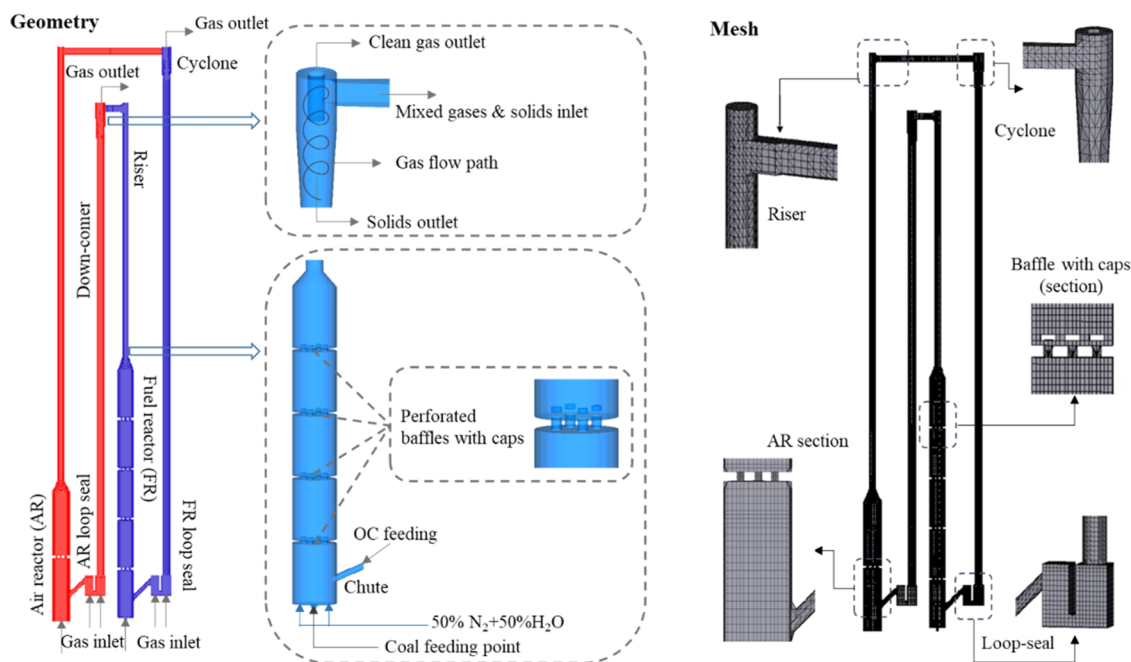


Figure 2. Schematic view of the multistage interconnected fluidized bed reactor.

Supporting Information, as summarized from the work of Parker et al.²⁶ The bubble-based EMMS model was applied as a drag model in the simulation by considering the effect of bubbles in the bubbling fluidized bed based on our previous study on the fluidization characteristics.²⁰

During the simulation of the CLC system with a multistage fluidized bed, coal was used as fuel and hematite was adopted as an oxygen carrier. When coal particles entered the FR, they would be pyrolyzed at high temperatures to produce char, volatiles, moisture, and ash. The char particles produced by coal pyrolysis would react with the gasification medium (H_2O and CO_2) in the FR to produce reducing gases, such as H_2 and CO . Meanwhile, combustible gases reacted with OC particles and the active component (Fe_2O_3) in OC was partially reduced to Fe_3O_4 because of the high oxygen to fuel ratio in the tests. Finally, if the char particles did not react entirely in the FR, they were very likely to be carried into the AR by the OC particles, which would be oxidized with O_2 in the AR to produce CO_2 . The reaction kinetics used in this work are summarized in Table S2 in the supporting information. These models were obtained from sources in the open literature.^{28–32}

2.2. Reactor Structure and Mesh. A schematic view of the multistage interconnected fluidized bed reactor simulated in this work is shown in Figure 2, where the dimension of the simulation model is the same as the experimental one.¹⁸ The unit consisted of a two-stage air reactor (AR), a five-stage fuel reactor (FR), and those connecting components, including risers, downcomers, loop seals, chutes, and cyclones. The coal feeding point was at the bottom of the FR, and the raw OC particles could be transmitted into the FR via the chute connected with the loop seal. The cyclone's structure was like a hollow cylinder, where particles could fall along the inner cylinder in a spiral path. Meanwhile, the clean gases blew out from the top of the cyclone, and the gas–solid separation could be achieved effectively. As to the grid setting on the magnified part in the device, the regular geometries, including risers, loop seals, and downcomers, were meshed with structured and dilute meshes. At the same time, the complex

structures like baffles in the FR and AR were simplified first and divided by delicate meshes. Three different grid resolutions were set to determine grid independency in the simulation.

2.3. Initial and Boundary Conditions. In the simulation, the no-slip boundary condition is used between the gas phase and the wall, while the bounce-back boundary condition is applied for the collision between the solid phase and the wall.^{33,34} The OC particle size distribution in the experiment was analyzed, as presented in Figure 3, which was imported

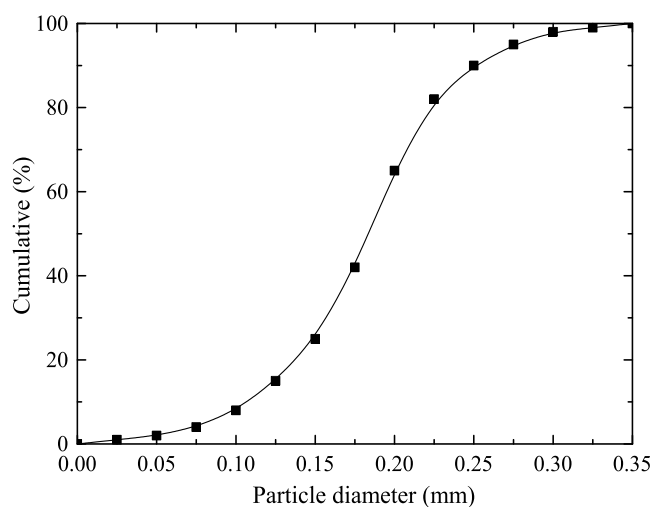


Figure 3. Particle size distribution of the hematite.

into the PSD file. The lignite coal was chosen as fuel, with an average size of 0.25 mm. Table 1 shows the proximate analysis of the lignite coal and the ultimate analysis of the combustible part. The composition of the hematite was necessary for the simulation, as shown in Table 2. Initially, the whole reactor was inundated with N_2 , and particles were packed in it with a close pack volume fraction of 0.6 at 850 °C. The initial packing

Table 1. Proximate and Ultimate Analyses of Lignite Coal

proximate analysis of coal (%)				ultimate analysis of V and FC (%)				
M	A	V	FC	C	H	O	N	S
19.16	16.5	35.53	28.81	45.39	3.85	16.95	0.98	1.45

Table 2. Chemical Analysis of Hematite in the Experiment and Simulation

composition	Fe ₂ O ₃	SiO ₂	Al ₂ O ₃	others
%	83.21	9.49	6.8	0.2

heights in the FR and AR were set as 0.7 and 0.36 m, respectively, based on the bed inventory in the experiment. The inlet gases in the FR bottom included 50% N₂ and 50% H₂O, with a flow rate of 0.35 m/s, while the gas flow rate in AR was set as 0.4 m/s, including 50% N₂ and 50% O₂. The coal particles were supplied through the coal feeding point at a feeding rate of 3.6 kg/h. The main physical parameters were selected according to previous research,^{35,36} where the particle–particle friction coefficient was 0.3 and the recovery coefficient was 0.9. The time step was set between 5×10^{-5} and 2.5×10^{-4} s, automatically adjusted according to the CFL number.

2.4. Data Evaluation. Three typical parameters were used to evaluate the performance in the thermal simulation on the multistage CLC reactor, including the CO₂ capture rate (η_{CC}), oxygen demand (Ω_{OD}), and combustion efficiency in the FR (η_{FR}). These parameters were obtained based on references from a previous review article.^{10–12}

Due to the inactivity of N₂ in the simulation, the molar flow of the outlet gases can be speculated by the inlet gas flow of N₂ and the fraction of each outlet gas ($i = \text{CO}, \text{CO}_2, \text{CH}_4, \text{H}_2$). It can be calculated as eq 1

$$q_{\text{out}}(i, t) = q_{\text{total}}(t) \cdot \varphi(i, t) = \frac{1}{22.4} \cdot \frac{q_{\text{in}}(\text{N}_2)}{\varphi(\text{N}_2)} \cdot \varphi(i, t) \quad (1)$$

where $q_{\text{out}}(i, t)$ (mol/s) is the molar flow rate of i species at t time at the FR outlet and $\varphi(i, t)$ is the fraction of i species at t time at the FR outlet.

The CO₂ capture rate (η_{CC}) is proposed to characterize the carbon capture ability of the CLC plant. It is defined as the fraction of carbon emitted as gases from the outlet of FR related to the total emission of carbonaceous gases from both AR and FR outlet, as shown in eq 2

$$\eta_{CC} = \frac{q_{C, \text{FR}}}{q_{C, \text{FR}} + q_{C, \text{AR}}} = \frac{[q_{\text{CO}_2} + q_{\text{CO}} + q_{\text{CH}_4}]_{\text{FR, out}}}{[q_{\text{CO}_2} + q_{\text{CO}} + q_{\text{CH}_4}]_{\text{FR, out}} + [q_{\text{CO}_2}]_{\text{AR, out}}} \quad (2)$$

where $q_{C, \text{FR}}$ and $q_{C, \text{AR}}$ are the molar flow rates of carbon at the FR and AR outlets, respectively, and $q_{\text{CO}_2, \text{AR}}$ is the molar flow rate of CO₂ at the AR outlet.

The oxygen demand (Ω_{OD}) is the fraction of oxygen required to fully oxidize the combustible gas in the FR exhaust gas to the oxygen needed for the complete conversion of the coal fed into the FR,¹² as shown in eq 3

$$\Omega_{OD} = \frac{[0.5 \cdot q_{\text{H}_2} + 0.5 \cdot q_{\text{CO}} + 2 \cdot q_{\text{CH}_4}]_{\text{FR, out}}}{n_{\text{O}_2, \text{ coal}}} \quad (3)$$

where $n_{\text{O}_2, \text{ coal}}$ (mol/s) is the oxygen needed for the complete conversion of coal.

The combustion efficiency in the FR (η_{FR} , %) is another index for evaluating the FR performance. It can be described by the oxygen demand, with the carbon burned in the AR being subtracted, as shown in eq 4

$$\eta_{FR} = \left(1 - \frac{[0.5 \cdot q_{\text{H}_2} + 0.5 \cdot q_{\text{CO}} + 2 \cdot q_{\text{CH}_4}]_{\text{FR, out}}}{n_{\text{O}_2, \text{ coal}} - n_{C, \text{ slip}}} \right) \times 100\% \quad (4)$$

where $n_{C, \text{ slip}}$ is the molar carbon flow to the AR.

In addition, the wall erosion³⁷ in the device was also considered in the CPF simulation. It is a function of particle mass, particle speed, and the angle at which particles strike the wall. The form of erosion is dependent on the wall materials. When enabled, the erosion model in the CPF simulation tracks the accumulated impacts of particles on each wall patch in the geometry. The magnitude of the impact value, I_p , is calculated for each particle as eq 5

$$I_p = \omega(\theta_p) \cdot m_p^a \cdot u_p^b \quad (5)$$

where m_p (kg/s) is the particle mass, u_p (m/s) is the particle speed, a and b are user-specified constants, and $\omega(\theta_p)$ is a weighting factor that is a function of the impact angle of attack θ_p .

3. RESULTS AND DISCUSSION

3.1. Model Validation. The computational model of the 3 kW_{th} multistage CLC reactor was validated by comparing the simulation results of pressure distribution in the axis of FR and the flue gas concentrations at the FR outlet with the experimental one. The previous study conducted a thermal experiment on this CLC system.¹⁷ Figure 4 compares the pressure distribution in the multistage FR between the

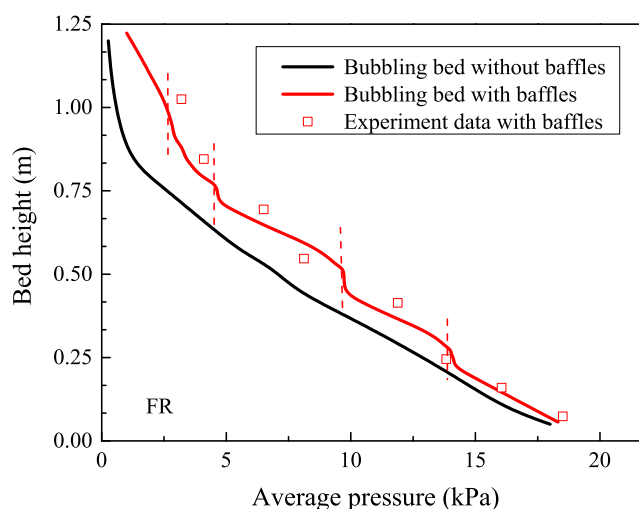


Figure 4. Model validation: simulated pressure and experimental pressure.

simulation and experiment. The pressure profile in a traditional bubbling bed without baffles is also shown as a control group. Compared with the pressure slope keeping a constant in the dense zone with height in the bubbling bed without baffles, the insert of perforated baffles made the pressure distribution profile step by step. The pressure curve seemed linear in each dense zone and dropped sharply in each dilute zone. Meanwhile, the pressure curve in the thermal simulation fit well with the experimental results, which revealed that the accuracy of the hydrodynamics based on this model was relatively high.

In addition, the gas products at the FR outlet were investigated to analyze the influence of grid number on the thermal simulation results, and the results are shown in Figure 5. It should be noted that the exhaust gas mole concentration

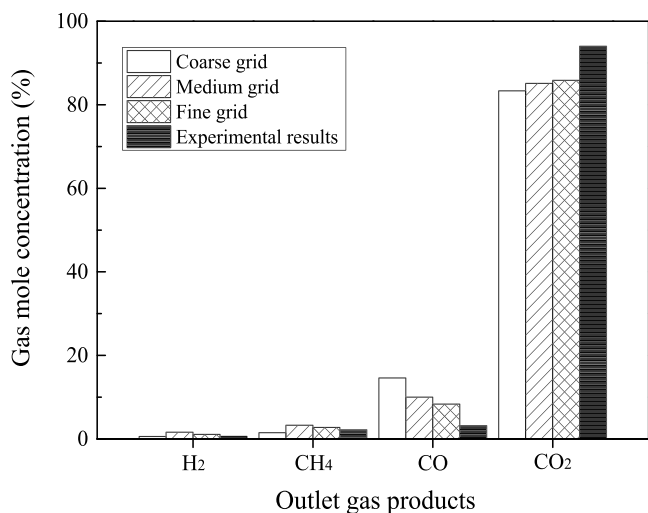


Figure 5. Effect of grid number on gas concentration distribution.

is on a dry basis, and N₂ is not considered in the calculation. The mole concentrations of both CH₄ and H₂ were lower than 5%, and the grid number (mesh size) slightly influenced the results. Among these results, the mole concentration of CO₂ was the most, arriving at about 80%. The deviations of the CO₂

gas concentration corresponding to the three grid numbers from the experimental results were 7.23, 4.32, and 4.29%, respectively. Hence, the simulation results would be more accurate with increasing the grid number, but the calculation time would increase accordingly. For accuracy of the computation results and cost of calculation time, a medium number of grids was used for the calculation in the thermal simulation.

3.2. Gas Distribution in the FR. In the performance of the CLC reactor, the outlet gas distribution is the basis for evaluating the reaction characteristics. Figure 6 presents the evolution of the gas mole fraction at the FR outlet during 60 s in the simulation. The mole fraction of CO₂ increased sharply to about 0.02 in the first 3 s of operation and then increased slowly. Its mole fraction curve fluctuated and finally stabilized at about 0.032. The yield of CH₄ was not high, and its mole fraction increased slightly from 0 to 0.001 in 0–3 s. In the first 3 s, CO and H₂ were hardly produced, and then the mole fraction of CO gradually increased to 0.005, while the H₂ mole fraction slowly rose to 0.001. The mole fraction curves of both gases showed apparent fluctuations after 15s, indicating that the water gas shift reaction began to work at this time. As to the fluidization gas N₂ and gasification gas H₂O in the right-hand figure, the mole fraction of N₂ decreased from 1.0 to about 0.85, and the mole fraction of H₂O increased from 0 to about 0.12 in the first 5s. All the gases reached a stable state after about 50s, indicating that the chemical reaction in the reactor reached dynamic equilibrium.

Figure 7 presents the evolution of the averaged gas mole concentration profile along the FR bed height. The process can be divided into three periods: pyrolysis, reduction, and stabilization. In the first period, coal particles were decomposed to combustible gases, including H₂, CH₄, and CO, where OC particles could not oxidize in time. The CO₂ concentration was as high as 50% in this period, while the CH₄ concentration was the smallest one maintaining about 10%. The existence of a homogeneous reaction made H₂, CO, and CO₂ concentration curves fluctuated slightly during this period. In the second period, the CO₂ concentration increased from 40% to about 90%, while the concentration of CO and H₂ decreased to 10 and 1%, respectively. Although the coal

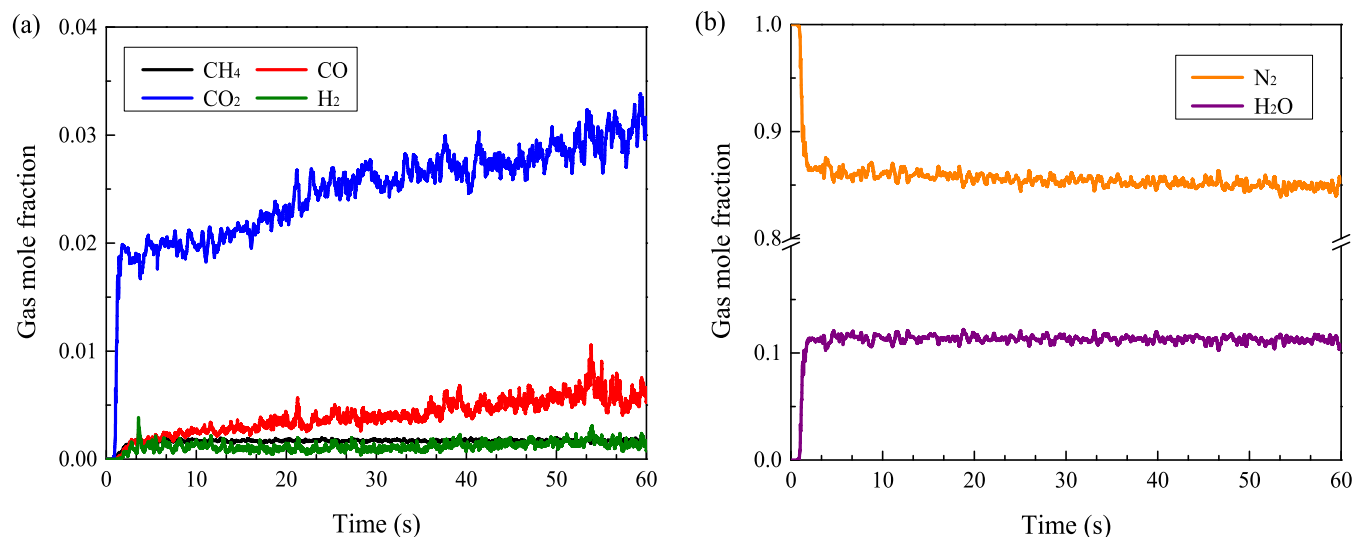


Figure 6. Evolution of gas mole fraction at the FR outlet: (a) H₂, CH₄, CO, and CO₂ and (b) N₂ and H₂O.

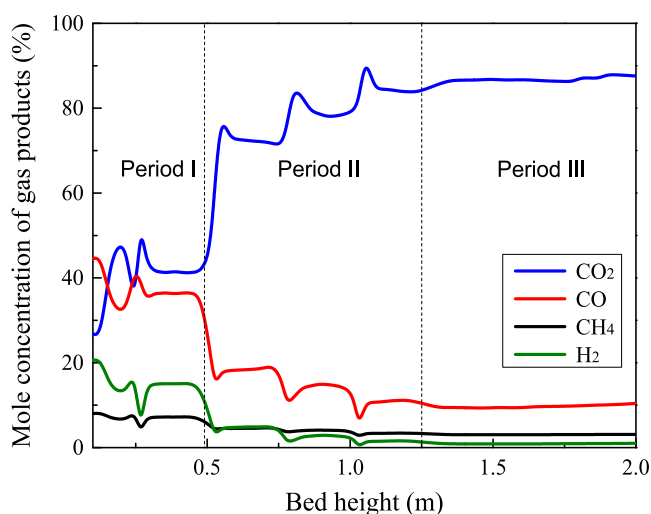


Figure 7. Gas mole concentration (H_2 , CH_4 , CO , and CO_2) along the FR bed height.

pyrolysis process was not completed in this period, the pyrolysis intensity was far lower than that in the first stage. The OC particles reacted with H_2 , CO , and CH_4 to produce a large amount of CO_2 . Compared with CO and H_2 , the activity in CH_4 was the smallest, so the decrease in CH_4 concentration was not evident. The stepped tendency of the other three gas concentration curves (H_2 , CO , and CO_2) was caused by the existence of baffles in the FR. The FR was divided into several independent and connected bubbling fluidized beds; thus, a CO_2 concentration peak existed in the dilute phase region of each chamber. Finally, the third period was located in the riser at the upper part of the FR. During this period, all of the gas concentration curves tended to be flat, and various reactions gradually entered the stable stage, where the concentrations of CO_2 , CO , H_2 , and CH_4 were maintained at about 90, 10, 0.5, and 1.5%, respectively.

3.3. Process Intensification in the FR. **3.3.1. Residence Time Distribution.** The residence time distribution (RTD) of particles in FR is one of the critical factors in determining the

gas–solid reaction. Hence, the RTDs of OC and char particles were studied, respectively, in the simulation with the individual FR within enough simulation time. The raw data of these two kinds of particles were obtained, as summarized in Figure 8. The percentage of OC particles between different residence time intervals is presented in Figure 8a, where most OC particles stayed in the FR for around 100–150 s in a visualized way. Approximately 80% of OC particles fluidized in the FR for more than 100 s, and the average particle residence time was 120 s. The reason was that the special baffles' structure in the multistage reactor hindered the upward transfer of some particles. Due to the high density and relatively large particle size, most of the OC particles were concentrated in the dense phase area of each chamber to ensure sufficient residence time. The fluidization number mainly affected the OC particles' residence time in the FR. The longer the residence time, the more adequate the OC reduction reaction, thus increasing the CO_2 concentration at the FR outlet. However, the RTD of char particles was different, as shown in Figure 8b. Most of the char particles (80%) in the FR concentrated ranged from 0 to 30 s, and the average char residence time was 23.13 s. The char gasification process was likely to be limited, and the main reason was that relatively violent gas–solid in the FR caused the elutriation of fine char particles. Due to its low density and small particle size, char particles were mainly concentrated in the upper area of each chamber, which was easy to be carried by the fluidization agent to the upper chamber. Hence, the RTD of char particles was mainly affected by the entrainment of OC particles, which was relatively lower in each chamber. The gasification reaction of char particles in the FR was insufficient, resulting in the reduction of gas combustion efficiency.

3.3.2. Particle Backmixing Rate. In the fluidization of a multistage fluidized bed, the particles impacted the baffles in the process of upward movement and part of them separated from upward particles and fell back due to inertia in each chamber, resulting in a particle backmixing condition, as shown in Figure 9a. The phenomenon helped strengthen the gas–solid contact and improve reaction efficiency. Hence, discussing the particle backmixing rate in each room is

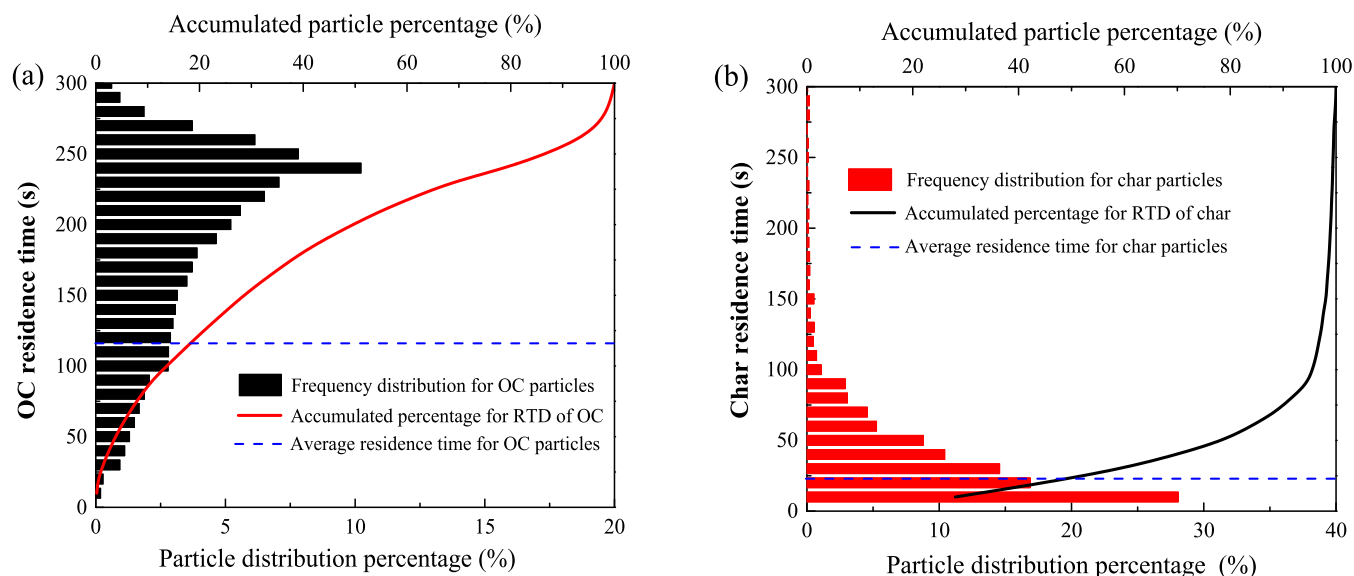


Figure 8. Particle residence time distribution in FR: (a) OC particles and (b) char particles.

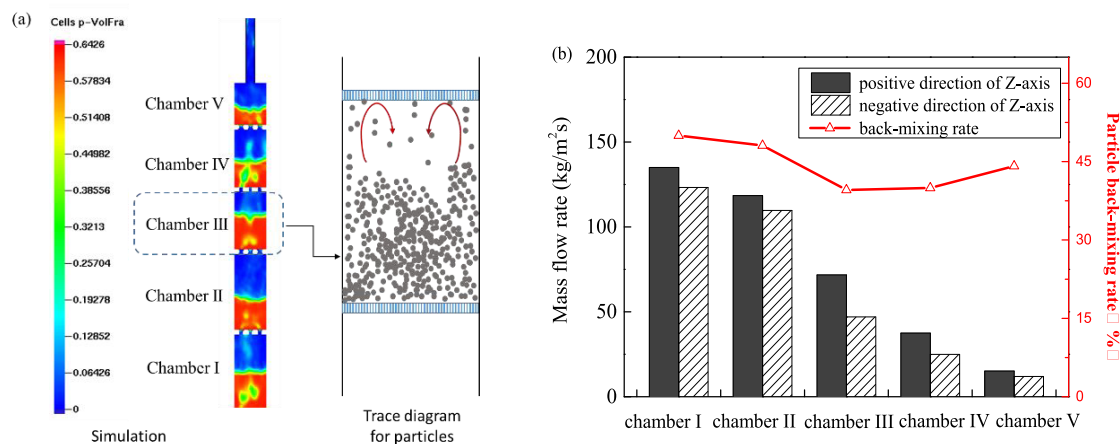


Figure 9. (a) Particle volume fraction in the FR and (b) particle backmixing rate in the FR.

significant. In the setting of simulation conditions, five flux planes, which can record the particle mass flow rate, were placed at the dilute phase of each chamber. When the fluidization was maintained stable, the mass flow through five flux planes between the 60 and 80 s intervals was recorded. The vertical axis of the FR was defined as the Z-axis. From the perspective of statistical significance, the mass flow in the positive direction of the Z-axis represented the mass flux of particles upward. In contrast, the mass flow in the negative direction represented the flux of particles falling back. Thus, the particle backmixing rate in each room can be described as the ratio of the backmixing flux to the total mass flux flowing through the plane in the paper, as shown in Figure 9b. We can see that the particle backmixing in the bottom chamber was the largest. With an increase of bed height, the particle mass transported upward showed a decreasing trend, and so as the particle backmixing mass. The reason was that plenty of particles concentrated in the lower three chambers, where more particles transmitted upward with the fluidization agent. Although the particle backmixing mass reduced with an increase in bed height, the backmixing rates of particles in each chamber remained at about 45 wt %. When the OC particles fell back due to baffles, they were in complete contact with the upward combustible gas in the dilute phase area in each chamber. This process was conducive to the sufficient reduction of OC particles and improved the fuel combustion efficiency in the FR. Meanwhile, the particles entering the upper chamber would not fall back to the lower chamber, which weakened the particle loss between chambers and was advantageous to stabilizing the circulation of solid particles in the fluidized bed.

3.3.3. Chemical Reaction Characteristics. The chemical reaction characteristics can be obtained by detecting the outlet gas concentration in the thermal simulation, including CO₂ capture rate, oxygen demand, and combustion efficiency in the FR. The reaction property data in the multistage CLC reactor are evaluated by eqs 1–4, and the results are summarized in Table 3. The CO₂ mole fraction at the outlet FR was as high as 93.8%, indicating that the prolonged OC residence time improved the reduction efficiency and transformed more combustible gases. In addition, the combustion efficiency in the FR was up to 90.2%, and the oxygen demand rate in the tower fuel reactor was only 3.8%. The possible reason was that the backmixing rate in the multistage FR was high, and large

Table 3. Chemical Reaction Characteristics in the Multistage CLC Reactor

reaction characteristics in the CLC process	CO ₂ mole fraction	combustion efficiency	oxygen demand	CO ₂ capture rate
%	93.8	90.2	3.8	80.3

bubbles were broken into small bubbles through internal baffles, which strengthened the gas–solid contact in the FR. However, due to the insufficient char residence time in the FR, the char particles cannot be gasified completely. These residual particles would enter the AR carried by OC particles, resulting in insufficient CO₂ capture capacity of the FR and the CO₂ capture rate was only 80.3%. Hence, it is necessary to optimize the reactor further to improve the CO₂ capture rate.

3.4. Wall Erosion in the System. Wall erosion is a significant problem in the operation of a circulating fluidized bed, which is usually caused by the severe hitting of particles on the heating surface at high temperatures.³⁵ The long-term impact was easy to cause potential safety hazards to the reactor and restricted the continuous operation. It is significant to understand erosion characteristics in industrial applications. In the CPFED simulation, the wall erosion data appears in GMV as the variable impact within the geometry. A common postprocessing technique is to create isosurfaces of the erosion index in GMV to show different levels of erosion in the device, as shown in Figure 10. The result shows that the most prominent part was the cyclone separator. In the conventional cyclone design, the inlet area was not large to ensure particle separation efficiency and decrease the sintering risk of the OC particles. When the particles were accelerated through the riser, the high-speed gas would directly wash and impact the cyclone's wall, resulting in inevitable erosion. In addition, a slight erosion also existed on the internal baffles in the FR. When the particles went through the baffles, the suddenly contracted aperture created an uneven velocity field, resulting in an increased particle velocity at the baffles. According to eq 5, the impact function of particles on the wall is directly proportional to the 3.5th power of the particle velocity, and the increase of particle velocity aggravates the wall erosion.

The cyclone's structure needs to be optimized and improved to relieve the wall erosion in the system. The erosion distribution diagram presented that the main erosion area was the inlet area of the cyclone. Hence, we increased the

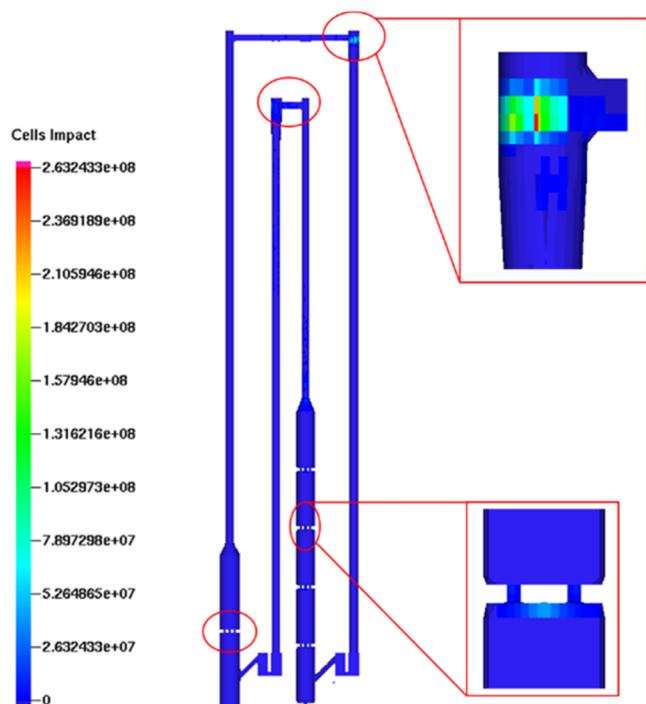
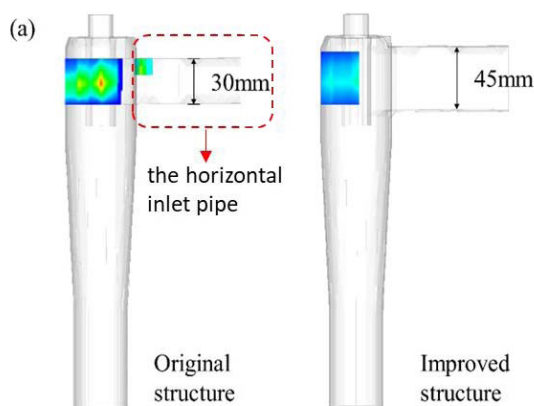


Figure 10. Wall erosion distribution in the multistage fluidized bed.

height of the horizontal pipe between the outlet riser and the cyclone separator cylinder. When the particles entered the hollow cylinder, their velocity was reduced. The wall erosion distribution on the cyclone was compared between the previous and the improved structure, as shown in Figure 11a. The improved one significantly reduced the erosion degree and severity of the inlet area to avoid the wear of the connecting pipe. To quantitatively describe the erosion on the cyclone separator, Figure 11b presents the curves of particle impact function on the wall along the radial direction of the cyclone tube under different inlet pipe heights. The height of the inlet pipe was changed from 30 to 45 mm, and the wall erosion was improved to a certain extent. For the operation optimization of the cyclone separator, there is a contradiction between the wall erosion rate and the separation efficiency. Although reducing the inlet velocity could relieve the wall erosion, the cyclone efficiency would be affected. According to the design criteria of the CFB cyclone, the improved inlet area



height should be lower than 0.75 times the cyclone's external cylinder diameter.

3.5. Optimization of the Loop Seal. The transient mass fraction of char particles in the multistage CLC reactor in the 60 s period was recorded in the simulation, as shown in Figure 12. Plenty of char particles were reacted and entrained by the

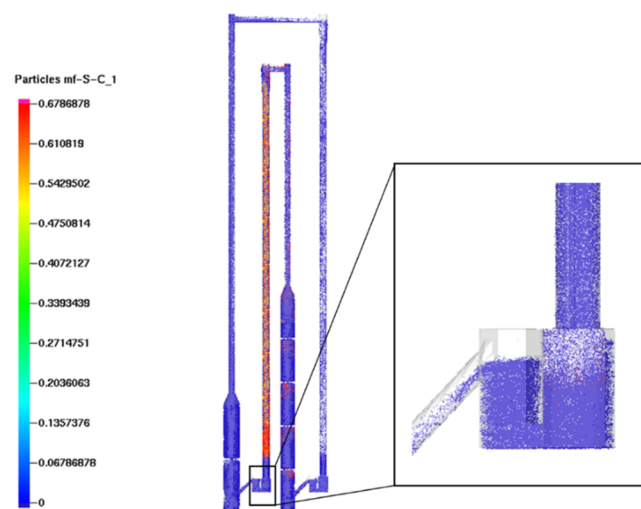


Figure 12. Transient mass fraction of char particles in the multistage CLC reactor.

OC stream to the upper chamber. Since the density of char particles is less than that of OC particles, a large number of char particles were suspended in the upper part of each chamber. The terminal velocity of char particles was lower, and they could be blown out more quickly. As we discussed above, the RTD of char particles was less than that of OC particles in the FR, so many residual char particles also appeared in the top chamber of FR. These char particles flew out of the riser, and plenty of them accumulated in the lower part of the downcomer, increasing the risk of entering into the AR.

The optimization of the AR loop seal was conducted to avoid the residual char particles transferred into the AR for a higher CO₂ capture rate. Figure 13a shows the original AR loop seal structure before improvement, which was a typical U-shaped structure for good sealing performance. N₂ is introduced into its bottom during operation to prevent particles from forming a dead zone. Figure 13b presents the

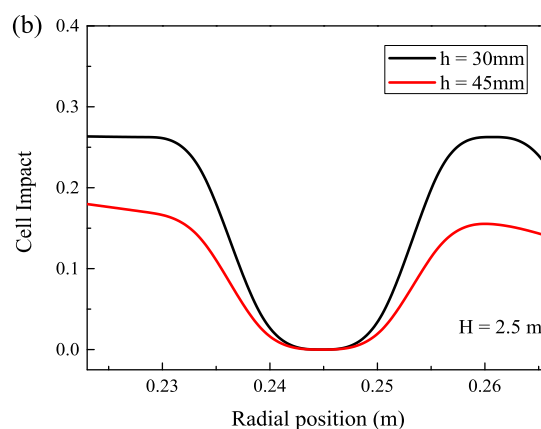


Figure 11. (a) Improvement on the horizontal pipe and (b) impact with different pipe heights.

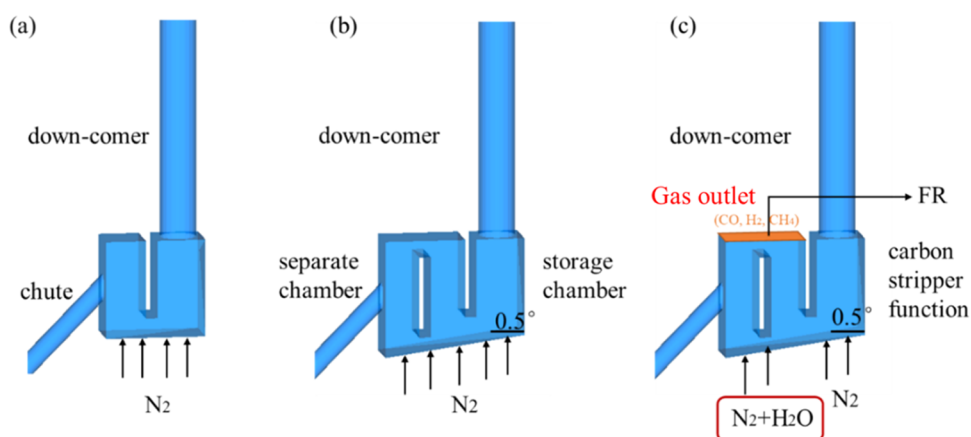


Figure 13. Optimization of the loop seal: (a) original structure, (b) improved structure, and (c) improved structure with a gasification agent.

improved AR loop seal. Based on the original structure, the LS widened the width and inclined the bottom plan by 0.5° , aiming at a smoother particle transformation. The AR loop seal was divided into a storage chamber and a separation chamber. In the left part of the separation chamber, an internal baffle was adopted in the middle to prevent char particles from entering the AR, hoping to realize the physical separation of char particles. In addition, to further intensify the residual char reaction, the AR loop seal was fluidized by $N_2 + H_2O$ at a low superficial velocity for char gasification. The gasification products were recycled back from the gas outlet to the FR again, as shown in Figure 13c. In the thermal operation, the temperature in the LS was usually set between 900 and 1000 °C for a higher gasification rate. There was probably erosion on the partition in the LS, but a method of steam cooling can be used to guarantee the baffle strength in the intended application.

The gas–solid flow process in the improved loop seal was simulated by the CPFDF method, and char particles were sent directly into the loop seal for precise observation. The char residence time in the supply chamber and downcomer of the AR loop seal was relatively long because they were fluidized by steam as a moving bed reactor. Figure 14 shows the distribution of particle species in the LS during the 60 s

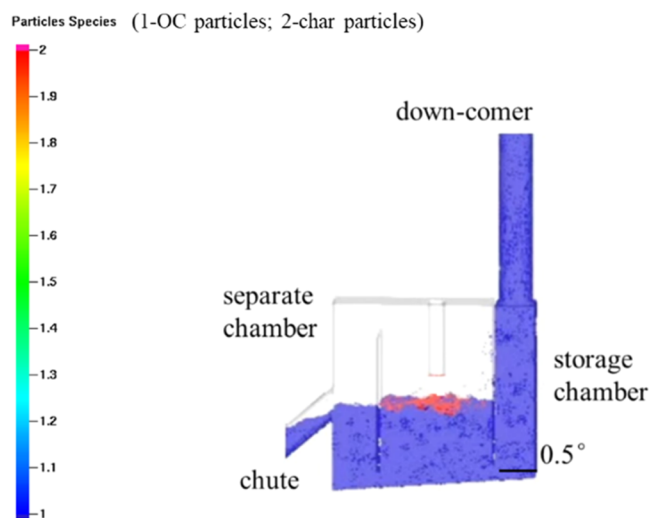


Figure 14. Particle species distribution in the improved loop seal.

operation. We can see that the transportation process of the reduced OC particles to the AR was stable and smooth, where the char particles were concentrated in the middle chamber and separated from the OC particles under the function of the baffle. Because of the low density, the char particles would float by the fluidization gas on the upper part of the separation chamber. The OC particles were transmitted to the leftmost chamber through the inclined bottom plane. In contrast, the char particles were blocked on the right side of the separation chamber and would not enter into the AR to realize the practical separation of these two particles.

The influence of the AR loop seal optimization on the CO_2 capture rate is shown in Figure 15. The change in the loop seal

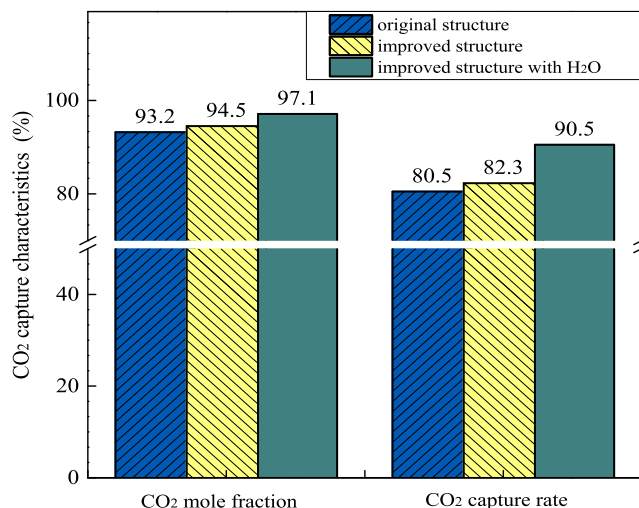


Figure 15. Influence of loop seal optimization on the CO_2 capture property.

structure can improve the CO_2 capture property, where the CO_2 mole fraction increased from 93.2 to 94.5%, and the CO_2 capture rate increased from 80.5 to 82.3%. When the LS bottom was accessed with a gasification agent, the produced combustible gases would be returned back to the FR. The AR loop seal here can function as a simple carbon stripper. Under this optimization method, the CO_2 capture rate increased to about 90.5%, further intensifying the CLC process in the laboratory-scale device.

3.6. Future Scale. It would be an extraordinary significance for the development of solid fuel CLC to erect a commercial

scale unit. The investigation of the multistage reactor at a laboratory level can guide the design of the MW_{th} boiler. Based on the heat and mass balance, the property of fuel and OC particles tested in the experiment can be used to calculate the circulation rate and bed inventory. According to the fluidization regimes in the FR and AR, the structural dimensions of the MW_{th} pilot can be obtained based on hydrodynamics. The results obtained from the multistage FR and the improved LS were prepared to understand the feasible optimization of a practical device. In addition, the practical application would simplify operation and increase the transferability to a commercial scale unit. A cooling system would be needed in the FR and loop seal.³⁸ Dilution effects with nitrogen should be avoided in the demonstration scale to increase the concentration of the target product CO₂ in the FR outlet.

4. CONCLUSIONS

A multistage interconnected CLC plant model coupled with the hydrodynamics and reactions was established. By comparing some results between the experiment and simulation, we found that the works on the simulation reflected the operation in a relatively accurate way. Some deviations may be attributed to setting limited reactions and simplifying the baffle in the simulation. By the optimization of adding baffles in the FR, the reaction process could be divided into three periods along the height, including the pyrolysis stage, reduction stage, and stabilization stage. In total, 80% of the OC particles stayed more than 100 s in the FR, where they can make complete contact with the upward gas, and the particle backmixing rate was about 45 wt %. Thanks to the strengthening effect of baffles on the gas–solid reaction, the oxygen demand rate was only 3.8%. However, the char residence time was less than 60 s, resulting in the reduction of CO₂ capture rate, which was only 80.3%. In addition, the erosion distribution on the fluidized bed wall was investigated, and the cyclone separator was the most prominent. Increasing the height of the horizontal pipe can relieve wall erosion. Finally, optimization on the loop seal reconstruction was conducted for a higher CO₂ capture rate. This method reduced the char particles entrained into the AR, and the combustible gas was resented to the FR. The CO₂ capture efficiency was increased to more than 90%. In our further study, more in-depth research on the design of an MW_{th} device will be carried out, for the purpose of promoting the improvement of carbon conversion in the industrial application.

■ ASSOCIATED CONTENT

SI Supporting Information

The Supporting Information is available free of charge at <https://pubs.acs.org/doi/10.1021/acsomega.2c04192>.

Governing equations of fluid/particles and the reaction kinetics of the model in the CPFD simulation (PDF)

■ AUTHOR INFORMATION

Corresponding Author

Laihong Shen – School of Energy and Environment, Southeast University, Nanjing 210096, China; orcid.org/0000-0003-1390-3631; Email: lhshen@seu.edu.cn

Authors

Xiao Zhu – Nanjing Vocational University of Industry Technology, Nanjing 210023, China

Rong Wang – Nanjing Vocational University of Industry Technology, Nanjing 210023, China

Tianxu Shen – School of Energy and Mechanical Engineering, Nanjing Normal University, Nanjing 210023, China

Complete contact information is available at:

<https://pubs.acs.org/10.1021/acsomega.2c04192>

Notes

The authors declare no competing financial interest.

■ ACKNOWLEDGMENTS

The authors acknowledge the support from the National Natural Science Foundation of China (Grant 52076044), the Natural Science Foundation of Jiangsu Province (Grant BK20220378), and the Natural Science Foundation of Jiangsu Provincial Colleges and Universities (Grant 22KJB470016).

■ ACRONYMS

ARair reactor
CCScarbon capture storage
CLCchemical looping combustion
CPFDcomputational particle fluid dynamics
FRfuel reactor
LSloop seal
OCoxygen carrier

■ REFERENCES

- (1) Yoro, K. O.; Daramola, M. O. CO₂ emission sources, greenhouse gases, and the global warming effect. *Adv. Carbon Capture* **2020**, 3–28.
- (2) Lyngfelt, A.; Abanades, J. C.; Anthony, E. J.; et al. Carbon capture and storage update. *Energy Environ. Sci.* **2014**, 7, 130–189.
- (3) Ishida, M.; Jin, H. A new advanced power-generation system using chemical-looping combustion. *Energy* **1994**, 19, 415–422.
- (4) Lyngfelt, A.; Leckner, B.; Mattisson, T. A fluidized-bed combustion process with inherent CO₂ separation application of chemical-looping combustion. *Chem. Eng. Sci.* **2001**, 56, 3101–3113.
- (5) Hossain, M. M.; Lasa, H. Chemical-looping combustion (CLC) for inherent CO₂ separations—A review. *Chem. Eng. Sci.* **2008**, 63, 4433–4451.
- (6) Dennis, J. S.; Scott, S. A.; Hayhurst, A. N. In situ gasification of coal using steam with chemical looping: a technique for isolating CO₂ from burning a solid fuel. *J. Energy Inst.* **2006**, 79, 187–190.
- (7) Markström, P.; Lyngfelt, A. Designing and operating a cold-flow model of a 100kW chemical-looping combustor. *Powder Technol.* **2012**, 222, 182–192.
- (8) Ma, J.; Zhao, H.; Tian, X.; et al. Chemical looping combustion of coal in a 5 kW_{th} interconnected fluidized bed reactor using hematite as oxygen carrier. *Appl. Energy* **2015**, 157, 304–313.
- (9) Lyngfelt, A.; Linderholm, C. Chemical-looping combustion of solid fuels—status and recent progress. *Energy Procedia* **2017**, 114, 371–386.
- (10) Adánez, J.; Abad, A.; Mendiara, T.; et al. Chemical looping combustion of solid fuels. *Prog. Energy Combust. Sci.* **2018**, 65, 6–66.
- (11) Song, T.; Shen, L. Review of reactor for chemical looping combustion of solid fuels. *Int. J. Greenhouse Gas Control* **2018**, 76, 92–110.
- (12) Ohlemüller, P.; Ströhle, J.; Epple, B. Chemical looping combustion of hard coal and torrefied biomass in a 1 MW_{th} pilot plant. *Int. J. Greenhouse Gas Control* **2017**, 65, 149–159.
- (13) Thon, A.; Kramp, M.; Hartge, E. U.; et al. Operational experience with a system of coupled fluidized beds for chemical looping combustion of solid fuels using ilmenite as oxygen carrier. *Appl. Energy* **2014**, 118, 309–317.

- (14) Pröll, T.; Kolbitsch, P.; et al. A novel dual circulating fluidized bed (DCFB) system for chemical looping processes. *AIChE J.* **2009**, *55*, 3255–3266.
- (15) Ma, J.; Tian, X.; Wang, C.; et al. Performance of a 50 kW_{th} coal-fueled chemical looping combustor. *Int. J. Greenhouse Gas Control* **2018**, *75*, 98–106.
- (16) Pérez-Vega, R.; Abad, A.; Garcia, L. F.; et al. Coal combustion in a 50 kW_{th} chemical looping combustion unit: seeking operating conditions to maximize CO₂ capture and combustion efficiency. *Int. J. Greenhouse Gas Control* **2016**, *50*, 80–92.
- (17) Markström, P.; Linderholm, C.; Lyngfelt, A. Chemical-looping combustion of solid fuels – design and operation of a 100kW unit with bituminous coal. *Int. J. Greenhouse Gas Control* **2013**, *15*, 150–162.
- (18) Lyngfelt, A.; Leckner, B. A 1000 MW_{th} boiler for chemical-looping combustion of solid fuels – Discussion of design and costs. *Appl. Energy* **2015**, *157*, 475–487.
- (19) Shen, T.; Wang, S.; Tian, H.; et al. Performance improvement of chemical looping combustion with coal by optimizing operational strategies in a 3kW_{th} interconnected fluidized bed. *Int. J. Greenhouse Gas Control* **2020**, *98*, No. 103060.
- (20) Zhu, X.; Shen, T.; George, B.; Shen, L. Design and operation of a multi-stage reactor system for chemical looping combustion process. *Fuel Process. Technol.* **2021**, *215*, No. 106748.
- (21) Andrews, M.; O'Rourke, P. The multiphase particle-in-cell (MP-PIC) method for dense particulate flows. *Int. J. Multiphase Flow* **1996**, *22*, 379–402.
- (22) Snider, D. M.; Clark, S.; O'Rourke, P. Eulerian–Lagrangian method for three-dimensional thermal reacting flow with application to coal gasifiers. *Chem. Eng. Sci.* **2011**, *66*, 1285–1295.
- (23) Fotovat, F.; Abbasi, A.; Spiteri, R. J.; et al. A CPFD model for a bubbly biomass–sand fluidized bed. *Powder Technol.* **2015**, *275*, 39–50.
- (24) Zhang, L.; Wang, Z.; Wang, Q.; et al. Simulation of oil shale semi-coke particle cold transportation in a spouted bed using CPFD method. *Powder Technol.* **2016**, *301*, 360–368.
- (25) Liu, H.; Li, J.; Wang, Q. Simulation of gas–solid flow characteristics in a circulating fluidized bed based on a computational particle fluid dynamics model. *Powder Technol.* **2017**, *321*, 132–142.
- (26) Parker, J. M. CFD model for the simulation of chemical looping combustion. *Powder Technol.* **2014**, *265*, 47–53.
- (27) Chen, X.; Ma, J.; Tian, X.; Wan, J.; Zhao, H. CPFD simulation and optimization of a 50 kW_{th} dual circulating fluidized bed reactor for chemical looping combustion of coal. *Int. J. Greenhouse Gas Control* **2019**, *90*, No. 102800.
- (28) Smoot, L.; Smith, P. *Coal Combustion and Gasification*; Plenum Press: New York, 1985.
- (29) Syamlal, M.; Bissett, L. *A.METC Gasifier Advanced Simulation (MGAS) Model*; N. P.: United States, 1992.
- (30) Bustamante, F.; Enick, R. M.; Cugini, A. V.; et al. High-temperature kinetics of the homogeneous reverse water-gas shift reaction. *AIChE J.* **2004**, *50*, 1028–1041.
- (31) Bustamante, F.; Enick, R. M.; Killmeyer, R. P.; et al. Uncatalyzed and wall-catalyzed forward water-gas shift reaction kinetics. *AIChE J.* **2005**, *51*, 1440–1454.
- (32) Abad, A.; Garcia-Labiano, F.; Diego, L. F.; et al. Reduction kinetics of Cu-, Ni-, and Fe-based oxygen carriers using syngas (CO + H₂) for chemical looping combustion. *Energy Fuels* **2007**, *21*, 1843–1853.
- (33) Galimov, A. Y.; Drew, D.; Lahey, J.; Moraga, F. The analysis of interfacial waves. *Nucl. Eng. Des.* **2005**, *235*, 1283–1292.
- (34) Harris, S. E.; Crighton, D. Solitons, solitary waves, and voidage disturbances in gas-fluidized beds. *J. Fluid Mech.* **1994**, *266*, 243–276.
- (35) Yin, S.; Zhong, W.; Jin, B.; et al. Modeling on the hydrodynamics of pressurized high-flux circulating fluidized beds by Eulerian–Lagrangian approach. *Powder Technol.* **2014**, *259*, 52–64.
- (36) Yan, J.; Lu, X.; et al. Validation and application of CPFD model in simulating gas-solid flow and combustion of a supercritical CFB boiler with improved inlet boundary conditions. *Fuel Process. Technol.* **2020**, *208*, No. 106512.
- (37) Xu, L.; Luo, K.; Zhao, Y.; et al. Multiscale investigation of tube erosion in fluidized bed based on CFD-DEM simulation. *Chem. Eng. Sci.* **2018**, *183*, 60–74.
- (38) Helbig, M.; Hilz, J.; Haaf, M.; Daikeler, A.; Ströhle, J.; Epple, B. Long-term carbonate looping testing in a 1 MW_{th} pilot plant with hard coal and lignite. *Energy Procedia* **2017**, *114*, 179–190.